Compressive Estimation of Wideband mmW Channel using Analog True-Time-Delay Array

Veljko Boljanovic and Danijela Cabric
Electrical and Computer Engineering Department, University of California, Los Angeles, CA, USA
Email: vboljanovic@ucla.edu, danijela@ee.ucla.edu

2021 IEEE Workshop on Signal Processing Systems (SiPS) | 978-1-6654-0144-9/21/$31.00 ©2021 IEEE | DOI: 10.1109/SiPS52927.2021.00038

***Abstract*—High-rate directional communication in millimeter-wave (mmW) systems requires a fast and accurate channel estimation. Novel array architectures and signal processing techniques are needed to avoid prohibitive estimation overhead associated with large antenna arrays. Recent advancements in hardware design helped the re-emergence of true-time-delay (TTD) arrays whose frequency-dependent beams can be leveraged for low-overhead channel probing and estimation. In this work, we consider an analog TTD array and develop a low-overhead compressive sensing based algorithm for channel estimation in frequency-domain. The algorithm is compared with related state-of-the-art approaches designed for analog phased antenna arrays. Our results reveal the advantages of the proposed TTD-based algorithm in terms of the required number of training symbols, estimation accuracy, and computational complexity.**

I. Introduction

Millimeter-wave (mmW) frequency bands offer abundant spectrum which has the key role in providing high data rates in modern wireless communication systems [1]. As shown in both theory and experiments, the base station (BS) and user equipment (UE) need to use large antenna arrays to combat severe path loss. Establishing a directional link between the BS and UE requires at least the knowledge of the dominant propagation direction obtained through beam training [2]. However, having the full channel knowledge provides additional benefits, including the ability to design optimal precoders and combiners, perform spatial multiplexing, allocate power optimally, determine the backup links to be used in the case of a link failure, and others. For this reason, mmW channel estimation techniques have been actively researched over the last several years.

Initial estimation algorithms were designed for frequency-flat mmW channels [3], [4]. However, practical mmW bandwiths are often wide, which motivated the development of estimation algorithms for frequency-selective channels [5]–[10]. The vast majority of the previous work considered arrays based on phase shifters at both the BS and UE. In particular, hybrid arrays with an analog front-end and a network of phase shifters is considered to be a promising architecture candidate for mmW systems due to its power efficiency. Most of previously designed digital signal processing (DSP) algorithms exploited the sparsity of mmW channels and formulated channel estimation as a compressive sensing (CS) problem in the time or frequency domain [5]–[8]. Different variations of matching pursuit algorithms were developed to recover the sparse vector in the CS problem, but many of them required a significant training overhead and computational resources for accurate estimation.

Here we consider an analog true-time-delay (TTD) array, which was previously shown to have low power consumption and good performance in mmW beam training [11], [12]. With its frequency-dependent beams, the analog TTD array can probe all angular directions simultaneously using different signal frequencies. In this work, we leverage the TTD frequency-dependent probing and design a CS-based DSP algorithm to estimate the channel. The algorithm is designed in the frequency domain and it is based on sub-band processing to reduce its complexity. We compare it with related state-of-the-art approaches in terms of the required number of training frames, estimation accuracy, and computational burden. To the best of our knowledge, this is the first paper to propose a wideband mmW channel estimation technique that leverages the properties of a TTD array.

The rest of the paper is organized as follows. In Sec. II, we present the system model and explain the CS-based problem formulation. In Sec. III, we explain the design of a TTD codebook and DSP algorithm. The comparison with the state-of-the-art approaches is presented in Sec. IV. Finally, Sec. V concludes the paper.

Scalars, vectors, and matrices are denoted by non-bold, bold lower-case, and bold upper-case letters, respectively. The (i, j)-th element and j-th column of $\mathbf{A}$ are denoted by $[\mathbf{A}]_{i,j}$ and $[\mathbf{A}]_{:,j}$, respectively. Conjugate, transpose, Hermitian transpose are denoted by $(.)^*$, $(.)^{\mathrm{T}}$, and $(.)^{\mathrm{H}}$, respectively. The Kronecker product of $\mathbf{A}$ and $\mathbf{B}$ is defined as $\mathbf{A} \otimes \mathbf{B}$.

II. System Model

We consider downlink estimation of mmW channel between a BS and a UE, which operate at the carrier frequency f_{c} using the bandwidth BW. The system uses a cyclic prefix (CP) based orthogonal frequency-division multiplexing (OFDM) waveform with M subcarriers that are loaded with binary phase shift keying (BPSK) symbols. The BS is equipped with a uniform linear fully connected hybrid array with N_{RF} radio frequency (RF) chains and N_{T} antennas. All N_{RF} degrees of freedom are exploited such that the BS sends a vector of symbols $\mathbf{x}[m] \in \mathbb{C}^{N_{\mathrm{RF}}}$ at the m-th subcarrier. The

This work was supported in part by NSF under grants 1718742 and 1955672. This work was also supported in part by the ComSenTer and CONIX Research Centers, two of six centers in JUMP, a Semiconductor Research Corporation (SRC) program sponsored by DARPA.

978-1-6654-0144-9/21/$31.00 ©2021 IEEE
DOI 10.1109/SiPS52927.2021.00038

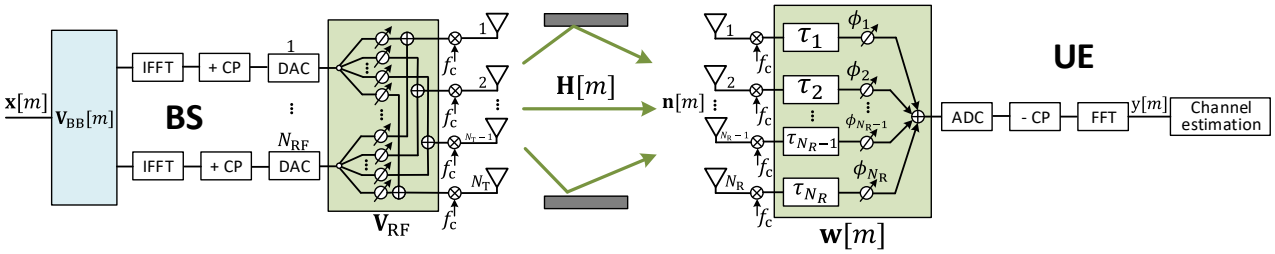

Fig. 1. Considered system model, where the BS is equipped with a fully connected hybrid analog-digital array and the UE with an analog TTD array.

vector $\mathbf{x}[m]$ is precoded using the matrix $\mathbf{V}[m] \in \mathbb{C}^{N_{\mathrm{T}} \times N_{\mathrm{RF}}}$, $\mathbf{V}[m] = \mathbf{V}_{\mathrm{RF}}\mathbf{V}_{\mathrm{BB}}[m]$, where $\mathbf{V}_{\mathrm{RF}} \in \mathbb{C}^{N_{\mathrm{T}} \times N_{\mathrm{RF}}}$ is a frequency-flat RF precoding matrix and $\mathbf{V}_{\mathrm{BB}}[m] \in \mathbb{C}^{N_{\mathrm{RF}} \times N_{\mathrm{RF}}}$ is a frequency-dependent baseband (BB) precoding matrix. The UE is assumed to have a uniform linear analog TTD array with N_{R} antennas, from which the signal is combined using the frequency-dependent RF combiner $\mathbf{w}[m] \in \mathbb{C}^{N_{\mathrm{R}}}$. Thus, the complex baseband signal at the m-th subcarrier is

$$y[m] = \mathbf{w}^{\mathrm{H}}[m]\mathbf{H}[m]\mathbf{V}_{\mathrm{RF}}\mathbf{V}_{\mathrm{BB}}[m]\mathbf{x}[m] + \mathbf{w}^{\mathrm{H}}[m]\mathbf{n}[m], \quad (1)$$

where $\mathbf{H}[m] \in \mathbb{C}^{N_{\mathrm{R}} \times N_{\mathrm{T}}}$ is the channel matrix and $\mathbf{n} \sim \mathcal{CN}\left(0, \sigma_{\mathrm{N}}^2 \mathbf{I}_{N_{\mathrm{R}}}\right)$ is the vector of complex white additive Gaussian noise at the m-th subcarrier. The considered system model is summarized and illustrated in Fig. 1.

A. Frequency-Selective Channel Model

We consider a geometric frequency selective channel model with L multipath components and N_{tap} delay taps. In the frequency domain, the channel for the m-th subcarrier can be expressed as follows

$$\mathbf{H}[m] = \sum_{l}^{L} G_l[m]\mathbf{a}_{\mathrm{R}}(\theta_l^{(\mathrm{R})})\mathbf{a}_{\mathrm{T}}^{\mathrm{H}}(\theta_l^{(\mathrm{T})}), \quad (2)$$

where $G_l[m] = \sum_{d=1}^{N_{\mathrm{tap}}} g_l p(dT_{\mathrm{s}} - \Gamma_l) e^{-j\frac{2\pi}{M}md}$ is the complex gain in the frequency domain. The function $p(\Gamma)$ models pulse shaping and other analog filtering, T_{s} is the sampling time, $g_l \in \mathbb{C}$ and $\Gamma_l \in \mathbf{R}$ are the complex gain and delay of the l-th path, respectively. The n-th element of the frequency-flat array response $\mathbf{a}_{\mathrm{R}}(\theta)$ is defined as $[\mathbf{a}_{\mathrm{R}}(\theta)]_n = \exp(-j(n-1)\pi\sin(\theta))$. The response $\mathbf{a}_{\mathrm{T}}(\theta)$ is defined in a similar way. The angles $\theta_l^{(\mathrm{R})} \in [-\pi/2, \pi/2)$ and $\theta_l^{(\mathrm{T})} \in [-\pi/2, \pi/2)$ are the angle of arrival (AoA) and angle of departure (AoD) of the l-th path. The channel in (2) can be written in a compact form as follows

$$\mathbf{H}[m] = \mathbf{A}_{\mathrm{R}}\mathbf{\Lambda}[m]\mathbf{A}_{\mathrm{T}}^{\mathrm{H}}, \quad (3)$$

where $\mathbf{\Lambda}[m]$ is a matrix with L non-zero values on the main diagonal that correspond to the gains $G_l[m]$, $\forall l$, and $\mathbf{A}_{\mathrm{T}} \in \mathbb{C}^{N_{\mathrm{T}} \times L}$ and $\mathbf{A}_{\mathrm{R}} \in \mathbb{C}^{N_{\mathrm{R}} \times L}$ are matrices of the spatial responses $\mathbf{a}_{\mathrm{T}}(\theta_l^{(\mathrm{T})})$, $\forall l$, at the BS and $\mathbf{a}_{\mathrm{R}}(\theta_l^{(\mathrm{R})})$, $\forall l$, at the UE, respectively. The expression in (3) can be approximated by using the matrices $\bar{\mathbf{A}}_{\mathrm{T}} = [\mathbf{a}_{\mathrm{T}}(\xi_1), ..., \mathbf{a}_{\mathrm{T}}(\xi_{Q_{\mathrm{T}}})]$ and $\bar{\mathbf{A}}_{\mathrm{R}} = [\mathbf{a}_{\mathrm{R}}(\xi_1), ..., \mathbf{a}_{\mathrm{R}}(\xi_{Q_{\mathrm{R}}})]$ of oversampled spatial responses in the following way

$$\mathbf{H}[m] \approx \bar{\mathbf{A}}_{\mathrm{R}}\bar{\mathbf{\Lambda}}[m]\bar{\mathbf{A}}_{\mathrm{T}}^{\mathrm{H}}, \quad (4)$$

where $\bar{\mathbf{\Lambda}}[m] \in \mathbb{C}^{Q_{\mathrm{R}} \times Q_{\mathrm{T}}}$ contains L channel gains $G_l[m]$, $\forall l$, as its non-zero elements. Commonly, $Q_{\mathrm{T}} \gg L$ and $Q_{\mathrm{R}} \gg L$, and the approximation error in (4) can be neglected.

B. Problem Formulation

Previously designed algorithms for compressive estimation of wideband mmW channels commonly considered the case where both the BS and UE utilize frequency-flat pseudo-random beamforming vectors [5], [6]. Such design of precoders and combiners was shown to reduce the DSP complexity as compressive measurements at all subcarriers can be modeled using one measurement matrix. In this work, we propose an *asymmetric* design where the BS uses frequency-flat pseudo-random precoders, while the UE relies on frequency-dependent TTD combiners. Specifically, we assume that the BS simultaneously transmits N_{RF} symbols $\mathbf{x}^{(t)}[m] \in \mathbb{C}^{N_{\mathrm{RF}}}$ defined as $\mathbf{x}^{(t)}[m] = \mathbf{q}^{(t)}s^{(t)}[m]$, where $\mathbf{q}^{(t)} \in \mathbb{C}^{N_{\mathrm{R}}}$ is a frequency-flat mapping vector [6] and $s^{(t)}[m]$ is a known BPSK symbol at the m-th subcarrier, in the t-th training frame. The vector $\mathbf{x}^{(t)}[m]$ is precoded using a frequency-flat precoding matrix $\mathbf{V}^{(t)} \in \mathbb{C}^{N_{\mathrm{T}} \times N_{\mathrm{RF}}}$, with each element defined as $e^{j\alpha}$, where α is drawn randomly from the uniform distribution $\mathcal{U}(0, 2\pi)$. At the UE side, the signal is combined using a frequency-dependent TTD combiner $\mathbf{w}^{(t)}[m]$. Thus, the received signal at the m-th subcarrier in the t-th training frame can be expressed as

$$y^{(t)}[m] = \mathbf{w}^{(t)\mathrm{H}}[m]\mathbf{H}[m]\mathbf{V}^{(t)}\mathbf{q}^{(t)}s^{(t)}[m] + \bar{n}^{(t)}[m]. \quad (5)$$

The post-combining noise is defined as $\bar{n}^{(t)}[m] = \mathbf{w}^{(t)\mathrm{H}}[m]\mathbf{n}^{(t)}[m]$. The effect of the BPSK symbol in (5) can be canceled by multiplying the received samples with $(s^{(t)}[m])^{-1}$. Using the result in (4), (5) can be vectorized as

$$y^{(t)}[m] = \mathbf{F}^{(t)}[m]\mathbf{A}\boldsymbol{\lambda}[m] + \bar{n}^{(t)}[m], \quad (6)$$

where $\mathbf{F}^{(t)}[m] \in \mathbb{C}^{1 \times N_{\mathrm{T}}N_{\mathrm{R}}}$ is a sensing matrix defined as $\mathbf{F}^{(t)}[m] = \mathbf{q}^{(t)\mathrm{T}}\mathbf{V}^{(t)\mathrm{T}} \otimes \mathbf{w}^{(t)\mathrm{H}}[m]$, $\mathbf{A} \in \mathbb{C}^{N_{\mathrm{T}}N_{\mathrm{R}} \times Q_{\mathrm{T}}Q_{\mathrm{R}}}$ is the dictionary defined as $\mathbf{A} = \bar{\mathbf{A}}_{\mathrm{T}}^{*} \otimes \bar{\mathbf{A}}_{\mathrm{R}}$, and $\boldsymbol{\lambda}[m] \in \mathbb{C}^{Q_{\mathrm{T}}Q_{\mathrm{R}}}$ is a sparse vector of channel gains obtained by stacking the columns of $\bar{\mathbf{\Lambda}}[m]$, i.e., $\boldsymbol{\lambda}[m] = \mathrm{vec}(\bar{\mathbf{\Lambda}}[m])$. Note that the vector $\boldsymbol{\lambda}[m]$ has the same support for any m, since the channel AoD-AoA pairs $(\theta_l^{(\mathrm{T})}, \theta_l^{(\mathrm{R})})$, $\forall l$, are common for all subcarriers. Assuming that the channel remains constant during the estimation process, after T training frames, the received samples can be vectorized in the following way

$$\mathbf{y}[m] = \mathbf{F}[m]\mathbf{A}\boldsymbol{\lambda}[m] + \bar{\mathbf{n}}[m], \quad (7)$$

where $\mathbf{y}[m] \in \mathbb{C}^{T}$, $\mathbf{y}[m] = [y^{(1)}[m], ..., y^{(T)}[m]]^{\mathrm{T}}$, $\mathbf{F}[m] \in \mathbb{C}^{T \times N_{\mathrm{T}}N_{\mathrm{R}}}$, $\mathbf{F}[m] = [\mathbf{F}^{(1)\mathrm{T}}[m], ..., \mathbf{F}^{(T)\mathrm{T}}[m]]^{\mathrm{T}}$, and $\bar{\mathbf{n}}[m] \in$

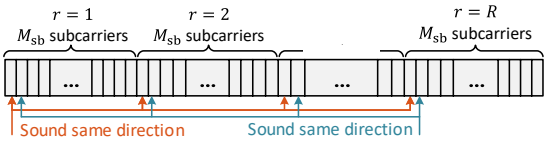

Fig. 2. An illustration of sub-bands. In each sub-band, M_{sb} subcarriers sound the entire angular range $[-\pi/2, \pi/2)$.

$\mathbb{C}^T$, $\bar{\mathbf{n}}[m] = [\bar{n}^{(1)}[m], ..., \bar{n}^{(T)}[m]]^{\text{T}}$. Based on (7), a sparse recovery problem for the m-th subcarrier can be defined as

$$\min \|\boldsymbol{\lambda}[m]\|_1 \quad \text{s.t.} \quad \|\mathbf{y}[m] - \mathbf{F}[m]\mathbf{A}\boldsymbol{\lambda}[m]\|_2^2 < \epsilon \qquad (8)$$

where ϵ is the maximum error power.

In this work, our goal is to design a low-complexity algorithm that solves (8). Specifically, we aim to design frequency-dependent TTD combiners $\mathbf{w}^{(t)}[m]$, $\forall t, m$, and a DSP algorithm that enable accurate channel estimation with a low computational burden and reduced training overhead compared to the state-of-the-art.

III. Proposed Channel Estimation Algorithm

In this section, we first describe the proposed design of TTD combiners $\mathbf{w}^{(t)}[m]$, $\forall t, m$, for channel estimation. Then we introduce a DSP algorithm that has a low computational complexity despite the fact that the UE uses frequency-dependent combiners.

A. Design of UE TTD Codebook

Frequency-dependent TTD codebooks were previously studied in [11], [12], for mmW beam training at the UE. The key idea was to sound the entire angular range $[-\pi/2, \pi/2)$ at once using different frequency components of the signal. This can be achieved by simultaneously mapping a subset of R uniformly selected subcarriers to each sounded direction [12]. In this work, we design a similar TTD codebook of pencil discrete Fourier transform (DFT) beams for channel estimation. It is worth noting that unlike beam training in [12], channel estimation requires the measurements at *all* M_{tot} OFDM subcarriers to be processed at the UE.

Based on the UE's array architecture in Fig. 1, the n-th element of the frequency-dependent TTD combiner $\mathbf{w}^{(t)}[m]$ is defined as follows [12]

$$\left[\mathbf{w}^{(t)}[m]\right]_n = \exp\left(-j\left(2\pi(f_m - f_{\text{c}})\tau_n + \phi_n^{(t)}\right)\right), \qquad (9)$$

where $f_m = f_{\text{c}} - \text{BW}/2 + (m-1)\text{BW}/(M_{\text{tot}}-1)$. The n-th delay tap τ_n is defined as $\tau_n = (n-1)\Delta\tau$, with $\Delta\tau$ being the delay difference between the neighboring antenna elements. The n-th phase tap $\phi_n^{(t)}$ is defined in a similar way as $\phi_n^{(t)} = (n-1)\Delta\phi^{(t)}$, where $\Delta\phi^{(t)}$ represents the phase difference between the neighboring antennas in the t-th training frame. The entire UE codebook of directional DFT beams can be set up with a proper design of $\Delta\tau$ and $\Delta\phi^{(t)}$, $\forall t$.

As in [12], we design the delay taps τ_n, $\forall n$, such that R subcarriers are mapped to each sounded direction in the t-th training frame. We first divide the bandwidth into R sub-bands of $M_{\text{sb}} = M_{\text{tot}}/R$ subcarriers, as illustrated in Fig. 2. In each sub-band, M_{sb} subcarriers should be associated with M_{sb} distinct DFT beams that sound the entire angular range.

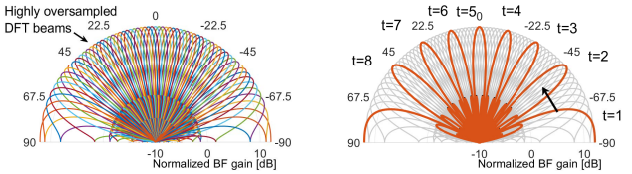

(a) (b)

Fig. 3. An example of the designed UE codebook with $N_{\text{R}} = 16$, BW = 2GHz, $M_{\text{tot}} = 1024$, $R = 16$, and $T = 8$. (a) Complete codebook with $\Delta\phi^{(t)} = 0$ and $O = 4$. (b) Rotations for first subcarriers in all sub-bands.

In [12], we showed that such DFT beams can be created by using $\Delta\tau = R/\text{BW}$, i.e., designing the delay taps as

$$\tau_n = (n-1)R/\text{BW}, \quad n = 1, ..., N_{\text{R}}. \qquad (10)$$

The taps in (10) ensure that all first subcarriers in R sub-bands sound the same direction, all second subcarriers sound the same, etc. An example of the resulting codebook with $\Delta\phi^{(t)} = 0$ in the t-th training frame is provided in Fig. 3(a). Note that if $M_{\text{sb}} > N_{\text{R}}$, the UE codebook consists of spatial DFT beams oversampled by the factor of $O = M_{\text{sb}}/N_{\text{R}}$.

To provide additional diversity and enable all M_{tot} subcarriers to sound multiple directions, it is necessary to rotate the TTD codebook in consecutive training frames using the phase shifters. We propose a uniform rotation of $2\pi/T$ rad in each training frame. Thus, $\Delta\phi^{(t)} = (t-1)2\pi/T$ and the corresponding phase taps are designed as

$$\phi_n^{(t)} = (n-1)(t-1)2\pi/T, \; n = 1, ..., N_{\text{R}}, \; t = 1, ..., T. \qquad (11)$$

The phase taps in (11) are frequency-flat, i.e., they are applied to all subcarriers equally. The codebook rotation is illustrated in Fig. 3(b) for the first subcarriers in all R sub-bands.

In the next subsection, we describe a DSP algorithm that leverages the designed frequency-dependent TTD codebook to solve the sparse recovery problem in (8).

B. OMP-based DSP Algorithm

Previous work on wideband mmW channel estimation considered various iterative greedy algorithms to solve (8), including the Orthogonal Matching Pursuit (OMP) [5], [6]. However, the majority of previous OMP variations relies on iterative estimation of channel angles and gains through per-subcarrier DSP, which significantly increases the computational complexity. Here we propose an OMP-based algorithm with sequential estimation of channel angles and gains. The algorithm first identifies the AoDs and AoAs using per-sub-band processing, and then it estimates the channel gains in a single iteration, which reduces the computational burden.

Assuming that M_{sb} subcarriers within each sub-band r have the same channel gains, the problem in (8) can be defined for all R sub-bands. Let $\boldsymbol{\lambda}_r \in \mathbb{C}^{Q_{\text{T}}Q_{\text{R}}}$ be a sparse vector of channel gains in the r-th sub-band. The vectors $\boldsymbol{\lambda}_r$, $\forall r$, have the same support as $\boldsymbol{\lambda}[m]$, $\forall m$. Let $\mathbf{F}^{(t)} \in \mathbb{C}^{M_{\text{sb}} \times N_{\text{T}}N_{\text{R}}}$ be the sensing matrix for each of the R sub-bands in the t-th training frame, defined as $\mathbf{F}^{(t)} = [\mathbf{F}^{(t)\text{T}}[1], ..., \mathbf{F}^{(t)\text{T}}[M_{\text{sb}}]]^{\text{T}}$. Note that all sub-bands can have a common sensing matrix $\mathbf{F}^{(t)}$ because of the codebook design in Section III-A, which ensured that the subcarriers $m = 1, ..., M_{\text{sb}}$, from the first

Algorithm 1 Proposed channel estimation algorithm

Inputs: $\mathbf{y}[m], \forall m, \quad \mathbf{y}_r, \forall r, \quad \mathbf{\Phi}, \quad \gamma, \quad \sigma_{\mathrm{N}}^2$
Initialize: $\mathbf{z}_r = \mathbf{y}_r, \forall r, \quad \Omega = \{\emptyset\}$
Calculate: $E = \frac{1}{TM_{\mathrm{tot}}} \sum_{r=1}^{R} \|\mathbf{z}_r\|_2^2$
Calculate: $E_{\mathrm{s}} = \frac{1}{TM_{\mathrm{tot}}} \sum_{r=1}^{R} \|\mathbf{y}_r\|_2^2 - \sigma_{\mathrm{N}}^2$
Calculate: $\epsilon = \gamma E_{\mathrm{s}} + \sigma_{\mathrm{N}}^2$
while $E > \epsilon$ **do**
  Estimate: $j^* = \mathrm{argmax}_j \sum_{r=1}^{R} \left| \left[\mathbf{\Phi}^{\mathrm{H}} \mathbf{z}_r \right]_j \right|^2$
  Update: $\Omega = \Omega \cup j^*$
  Estimate: $\hat{\boldsymbol{\lambda}}_r = \left([\mathbf{\Phi}]_{:,\Omega}^{\mathrm{H}} [\mathbf{\Phi}]_{:,\Omega} \right)^{-1} [\mathbf{\Phi}]_{:,\Omega}^{\mathrm{H}} \mathbf{y}_r, \quad \forall r$
  Update: $\mathbf{z}_r = \mathbf{y}_r - [\mathbf{\Phi}]_{:,\Omega} \hat{\boldsymbol{\lambda}}_r, \quad \forall r$
  Update: $E = \frac{1}{TM_{\mathrm{tot}}} \sum_{r=1}^{R} \|\mathbf{z}_r\|_2^2$
end while
Est.: $\hat{\boldsymbol{\lambda}}[m] = \left([\mathbf{\Phi}]_{\Psi,\Omega}^{\mathrm{H}} [\mathbf{\Phi}]_{\Psi,\Omega} \right)^{-1} [\mathbf{\Phi}]_{\Psi,\Omega}^{\mathrm{H}} \mathbf{y}[m], \quad \forall m$
where $\Psi = \{m' \mid m' = \mathrm{mod}(m, M_{\mathrm{sb}}) + (t-1)M_{\mathrm{sb}},\ t = 1, ..., T\}$
Outputs: $\hat{\boldsymbol{\lambda}}[m], \forall m, \quad \Omega$

sub-band ($r = 1$) sound the same directions as their counterparts from other sub-bands ($r > 1$). Let $\bar{\mathbf{n}}_r^{(t)} \in \mathbb{C}^{M_{\mathrm{sb}}}$ be the noise vector at the subcarriers in the r-th sub-band. Then, after T training frames and vectorization, the received signal $\mathbf{y}_r \in \mathbb{C}^{TM_{\mathrm{sb}}}$ in the r-th sub-band can be expressed as

$$\mathbf{y}_r = \mathbf{F}\mathbf{A}\boldsymbol{\lambda}_r + \bar{\mathbf{n}}_r, \tag{12}$$

where $\mathbf{F} \in \mathbb{C}^{TM_{\mathrm{sb}} \times N_{\mathrm{T}} N_{\mathrm{R}}}$ is $\mathbf{F} = [\mathbf{F}^{(1)\mathrm{T}}, ..., \mathbf{F}^{(T)\mathrm{T}}]^{\mathrm{T}}$, $\bar{\mathbf{n}}_r \in \mathbb{C}^{TM_{\mathrm{sb}}}$ is $\bar{\mathbf{n}}_r = [\bar{\mathbf{n}}_r^{(1)\mathrm{T}}, ..., \bar{\mathbf{n}}_r^{(T)\mathrm{T}}]^{\mathrm{T}}$. For conciseness, we introduce the effective measurement matrix $\mathbf{\Phi} \in \mathbb{C}^{TM_{\mathrm{sb}} \times Q_{\mathrm{T}} Q_{\mathrm{R}}}$, defined as $\mathbf{\Phi} = \mathbf{F}\mathbf{A}$. Similar as in (8), a sparse recovery problem for sub-band r can be formulated as follows

$$\min \|\boldsymbol{\lambda}_r\|_1 \quad \text{s.t.} \quad \|\mathbf{y}_r - \mathbf{\Phi}\boldsymbol{\lambda}_r\|_2^2 < \epsilon. \tag{13}$$

We propose to solve the problem in (13) using an iterative algorithm. In each iteration, it identifies the index of one non-zero value in $\boldsymbol{\lambda}_r, \ \forall r$, i.e., AoD-AoA pair of one propagation path, and then it refines all approximate channel gains jointly. In the first iteration, an AoD-AoA pair index is estimated by jointly considering all R sub-bands and calculating the correlation between $\mathbf{\Phi}$ and residuals $\mathbf{z}_r = \mathbf{y}_r, \ \forall r$, as follows

$$j^* = \underset{j}{\mathrm{argmax}} \sum_{r=1}^{R} \left| \left[\mathbf{\Phi}^{\mathrm{H}} \mathbf{z}_r \right]_j \right|^2. \tag{14}$$

Let the set $\Omega = \{j^*\}$ be the current estimate of the channel support. The approximated channel gains $\boldsymbol{\lambda}_r, \ \forall r$, are then estimated using least squares in the following way

$$\hat{\boldsymbol{\lambda}}_r = \left([\mathbf{\Phi}]_{:,\Omega}^{\mathrm{H}} [\mathbf{\Phi}]_{:,\Omega} \right)^{-1} [\mathbf{\Phi}]_{:,\Omega}^{\mathrm{H}} \mathbf{y}_r. \tag{15}$$

The channel support Ω and gains $\hat{\boldsymbol{\lambda}}_r, \ \forall r$, are used to subtract the contribution of the estimated propagation path from the measurements $\mathbf{y}_r, \ \forall r$, and obtain the corresponding measurement residuals for the next iteration. Mathematically, the residuals $\mathbf{z}_r, \ \forall r$, are calculated as

$$\mathbf{z}_r = \mathbf{y}_r - [\mathbf{\Phi}]_{:,\Omega} \hat{\boldsymbol{\lambda}}_r. \tag{16}$$

The algorithm iterates until a stopping criterion is satisfied. Using a predetermined number of iteration is impractical because the number of propagation paths in the channel is usually unknown. Thus, we propose the use of a stopping criterion based on the average subcarrier power E in the residuals $\mathbf{z}_r, \ \forall r$, calculated as follows [5], [6]

$$E = \frac{1}{TM_{\mathrm{tot}}} \sum_{r=1}^{R} \|\mathbf{z}_r\|_2^2. \tag{17}$$

When power in (17) falls below the threshold ϵ, the algorithm stops. It was shown in [6] that the optimal threshold for algorithms based on per-subcarrier processing is $\epsilon = \sigma_{\mathrm{N}}^2$, assuming that the noise variance σ_{N}^2 is known at the receiver. Unlike in [6], our proposed algorithm yields approximate channel gains $\boldsymbol{\lambda}_r, \ \forall r$, and consequently different residuals $\mathbf{z}_r, \ \forall r$, than algorithms with per-subcarrier processing, which creates the need for a different ϵ. At the subcarrier level, the current estimate of $\mathbf{y}[m]$ in (7) can be expressed as

$$\hat{\mathbf{y}}[m] = [\mathbf{\Phi}]_{\Psi,\Omega} \hat{\boldsymbol{\lambda}}_r + \underbrace{[\mathbf{\Phi}]_{\Psi,\Omega} \boldsymbol{\lambda}_e[m]}_{\text{Approx. error}}, \tag{18}$$

where $\Psi = \{m' \mid m' = \mathrm{mod}(m, M_{\mathrm{sb}}) + (t-1)M_{\mathrm{sb}},\ t = 1, ..., T\}$, $\hat{\boldsymbol{\lambda}}_r$ is the estimate of channel gains in the corresponding sub-band, and $\boldsymbol{\lambda}_e[m]$ is the channel gain error vector at the m-th subcarrier. For mathematical tractability, we treat $\boldsymbol{\lambda}_e[m]$ as a zero-mean random vector that is independent and identically distributed across different subcarriers. Let σ_{A}^2 be the variance of each element in the approximation error $[\mathbf{\Phi}]_{\Psi,\Omega} \boldsymbol{\lambda}_e[m]$. Then it is straightforward to show that the stopping threshold should be set as $\epsilon = \sigma_{\mathrm{A}}^2 + \sigma_{\mathrm{N}}^2$. However, the distribution of channels gains is unknown in general, which makes the estimation of σ_{A}^2 challenging. Thus, we estimate σ_{A}^2 numerically in Section IV as a fraction γ of the initial *useful* signal power E_{s} in a multipath channel, i.e., $\sigma_{\mathrm{A}}^2 = \gamma E_{\mathrm{s}}$, where E_{s} is defined as

$$E_{\mathrm{s}} = \frac{1}{TM_{\mathrm{tot}}} \sum_{r=1}^{R} \|\mathbf{y}_r\|_2^2 - \sigma_{\mathrm{N}}^2. \tag{19}$$

After stopping, the iterative algorithm outputs the channel support estimate Ω and dismisses the approximate channel gain estimates $\boldsymbol{\lambda}_r, \ \forall r$. Using Ω and (7), the channel gains are estimated for each subcarrier in a single iteration as follows

$$\hat{\boldsymbol{\lambda}}[m] = \left([\mathbf{\Phi}]_{\Psi,\Omega}^{\mathrm{H}} [\mathbf{\Phi}]_{\Psi,\Omega} \right)^{-1} [\mathbf{\Phi}]_{\Psi,\Omega}^{\mathrm{H}} \mathbf{y}[m], \tag{20}$$

where the set Ψ is defined as earlier. The proposed channel estimation algorithm is summarized in Algorithm 1.

IV. Comparison with State of the Art

In this section, we numerically evaluate the proposed OMP-based algorithm with per-sub-band processing. We also compare it with related state-of-the-art algorithms designed for arrays based on phase shifters, including the plain OMP algorithm in [5] and Simultaneous Weighted OMP (SW-OMP) algorithm proposed in [6]. The algorithms are compared in terms of required number of training frames, channel estimation accuracy, and computational complexity.

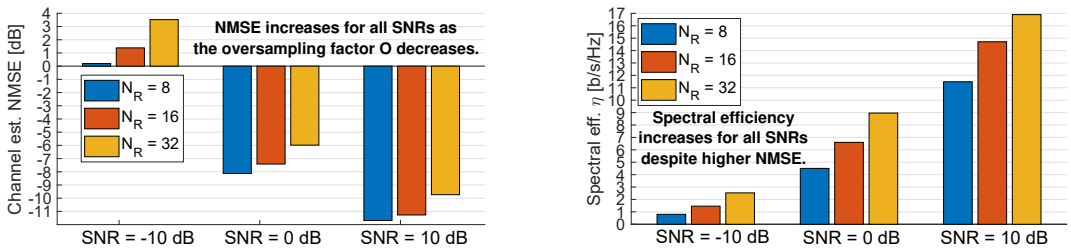

(a) (b)

Fig. 4. Performance of the algorithm for different sizes of the UE TTD array in terms of: (a) NMSE and (b) post-estimation spectral efficiency η.

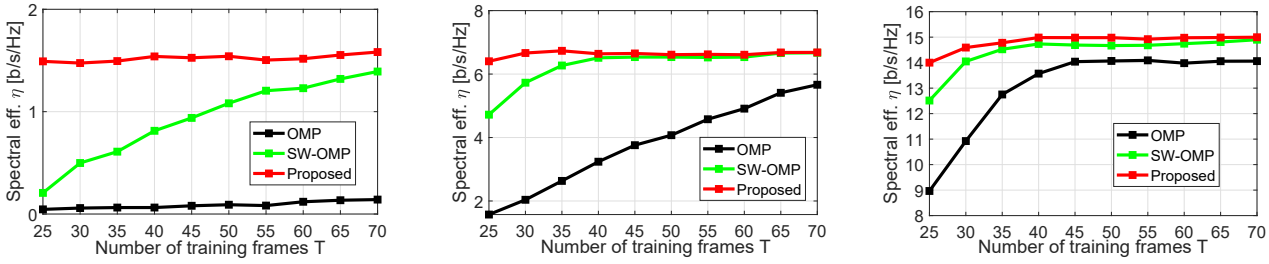

(a) (b) (c)

Fig. 5. Comparison with state-of-the-art algorithms in terms of required number of training frames T for the same spectral efficiency η in different SNR scenarios: (a) SNR $= -10$ dB, (b) SNR $= 0$ dB, and (c) SNR $= 10$ dB.

We consider a system with the carrier frequency $f_c = 28$ GHz, bandwidth BW $= 1$ GHz, $M_{\text{tot}} = 1024$ subcarriers, and $N_{\text{T}} = 64$ antennas and $N_{\text{RF}} = 4$ RF chains at the BS. The algorithm considers $R = 16$ sub-bands, while the number of spatial responses at the BS and UE is $Q_{\text{T}} = Q_{\text{R}} = 256$. The channel consists of $N_{\text{tap}} = 4$ taps and $L = 3$ paths with identically distributed gains $\alpha_i = \mathcal{CN}(0, \sigma_\alpha^2)$, $\forall i$. The SNR is defined as $\text{SNR} \triangleq L\sigma_\alpha^2/\sigma_{\text{N}}^2$.

We first numerically study a proper configuration of the power fraction parameter γ, assuming that $N_{\text{R}} = 16$ and $T = 35$. In simulations, the parameter γ is swept in the range $[0.05, 0.15]$. Our results indicate that the estimation accuracy increases with higher γ and thus it achieves the best performance with $\gamma = 0.15$. It is worth noting that the choice of γ is heavily influenced by the path gains α_i, $\forall i$. In certain non-line-of-sight scenarios with comparable path gains, a further increase of γ may severely deteriorate the performance by causing the algorithm to miss some significant paths. Thus, in this section, we assume the power fraction of $\gamma = 0.15$ to avoid potential performance degradation.

Next, we evaluate how the performance of the proposed TTD based channel estimation algorithm scales with the number of UE antennas N_{R} when the number of training frames is fixed to $T = 35$. We use two metrics, including the NMSE defined as

$$\text{NMSE} = \frac{\sum_{m=1}^{M_{\text{tot}}} ||\hat{\mathbf{H}}[m] - \mathbf{H}[m]||_F^2}{\sum_{m=1}^{M_{\text{tot}}} ||\mathbf{H}[m]||_F^2}, \tag{21}$$

where $\hat{\mathbf{H}}[m]$ is a channel estimate at the m-th subcarrier, and the average spectral efficiency defined as

$$\eta = \frac{1}{M_{\text{tot}}} \sum_{m=1}^{M_{\text{tot}}} \sum_{k=1}^{K_m} \log_2 \left(1 + \frac{|\hat{\mathbf{w}}_k^{\text{H}}[m]\mathbf{H}[m]\hat{\mathbf{v}}_k[m]|^2}{\sigma_{\text{N}}^2}\right) \tag{22}$$

where K_m is the rank of $\hat{\mathbf{H}}[m]$ and $\hat{\mathbf{w}}_k[m]$ and $\hat{\mathbf{v}}_k[m]$ are the k-th left and right singular vectors of $\hat{\mathbf{H}}[m]$, respectively. In Fig. 4(a), the NMSE is shown to increase with larger antenna arrays in all SNR regimes. Since T and M_{sb} are fixed, the number of measurements taken by $\mathbf{\Phi}$ is independent of N_{R}. However, an increase in N_{R} reduces the beam width and oversampling factor $O = M_{\text{sb}}/N_{\text{R}}$ of TTD combiners, which affects the channel estimation accuracy. Despite a higher NMSE, larger antenna arrays result in a higher post-estimation spectral efficiency due to more spatial degrees of freedom, as supported by the results in Fig. 4(b).

In Fig. 5, we assume $N_{\text{R}} = 16$ and compare the proposed algorithm with the state-of-the-art in terms of the required number of training frames T. The results indicate that the proposed algorithm requires a lower T for the same post-estimation spectral efficiency. The performance gap is especially noticeable with low overhead, where the proposed algorithm requires 5, 10, and 50 training frames less than the SW-OMP in high, medium, and low SNR regimes, respectively. The overhead savings are even bigger when the proposed approach is compared with the OMP algorithm.

Assuming $N_{\text{R}} = 16$ and $T = 35$, we compare the performance of the three algorithms across different SNR values in Fig. 6(a). The proposed TTD based algorithm achieves lower channel estimation NMSEs than the OMP and SW-OMP algorithms in medium and high SNR regimes by 8 dB and 3 dB, respectively. In a low SNR regime, the heuristic stopping criterion described in Sec. III-B may lead to an early termination of the proposed algorithm and thus a lower number of estimated paths and higher NMSE. However, the available support estimate is often more accurate than that of the OMP and SW-OMP algorithms, which results in an overall higher spectral efficiency, as previously shown for

TABLE I
COMPLEXITY OF PROPOSED AND STATE-OF-THE-ART OMP-BASED ALGORITHMS

Operation	Proposed algorithm	OMP from [5]	SW-OMP from [6]
Projection (j-th iter.)	$T_{\text{prop}} M_{\text{tot}}(Q_{\text{T}}Q_{\text{R}} - (j-1))$	$T_{\text{omp}} M_{\text{tot}}(Q_{\text{T}}Q_{\text{R}} - (j-1))$	$T_{\text{sw-omp}} M_{\text{tot}}(Q_{\text{T}}Q_{\text{R}} - (j-1))$
Maximum proj. (j-th iter.)	$R(Q_{\text{T}}Q_{\text{R}} - (j-1))$	$M_{\text{tot}}(Q_{\text{T}}Q_{\text{R}} - (j-1))$	$M_{\text{tot}}(Q_{\text{T}}Q_{\text{R}} - (j-1))$
Gain calculation (j-th iter.)	$j^3 + 2j^2 T_{\text{prop}} M_{\text{sb}} + jT_{\text{prop}} M_{\text{tot}}$	$j^3 M_{\text{tot}} + 2j^2 T_{\text{omp}} M_{\text{tot}} + jT_{\text{omp}} M_{\text{tot}}$	$j^3 + 2j^2 T_{\text{sw-omp}} + jT_{\text{sw-omp}} M_{\text{tot}}$
Residual update (j-th iter.)	$T_{\text{prop}} M_{\text{tot}}$	$T_{\text{omp}} M_{\text{tot}}$	$T_{\text{sw-omp}} M_{\text{tot}}$
Average power (j-th iter.)	$T_{\text{prop}} M_{\text{tot}}$	$T_{\text{omp}} M_{\text{tot}}$	$T_{\text{sw-omp}} M_{\text{tot}}$
Subcarrier gains (no iter.)	$J^3 M_{\text{sb}} + 2J^2 T_{\text{prop}} M_{\text{sb}} + JT_{\text{prop}} M_{\text{tot}}$	NA	NA

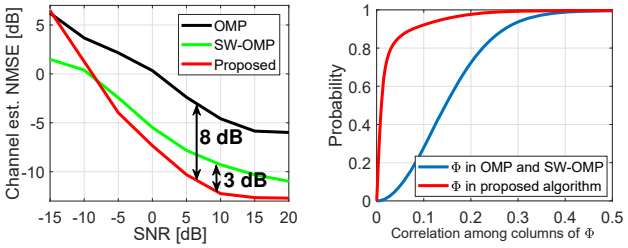

(a) (b)

Fig. 6. (a) Comparison with state-of-the-art algorithms in terms of the NMSE across different SNR values. (b) Cumulative distribution function of the correlation among the columns of the sensing matrix $\mathbf{\Phi}$.

SNR $= -10$ dB in Fig. 5(a). The reason for better support estimates is a lower correlation between the columns of the sensing matrix $\mathbf{\Phi}$ in the proposed algorithm than in the state-of-the-art approaches, as presented in Fig. 6(b). Due to the sub-band based processing, the columns of $\mathbf{\Phi}$ in the proposed algorithm belong to a much larger vector space, which consequently reduces the correlation among them.

In Table I, we summarized the complexity of the proposed and state-of-the-art algorithms. In the iterative part of the algorithm (first five operations in the table), the proposed approach achieves a lower computational complexity than the OMP and SW-OMP. The savings primarily come from the fact that the proposed approach requires a lower number of training frames, i.e., $T_{\text{prop}} < T_{\text{sw-omp}} < T_{\text{omp}}$, as discussed earlier. The AoD-AoA pair estimation in (14) consists of projections on the corresponding $\mathbf{\Phi}$, which is the most computationally expensive step in the algorithm, and search for the maximum value among projections. In the j-th iteration, the algorithm requires $(Q_{\text{T}}Q_{\text{R}} - (j-1))$ projections where the number of complex operations scales with $T_{\text{prop}} M_{\text{tot}}$. Finding the maximum projection on $\mathbf{\Phi}$ scales with the number of sub-bands R, instead of M_{tot} as in the OMP and SW-OMP algorithms. Similar computational savings as for projections are achieved for residual updates in (16) and average subcarrier power in (17), where the number of complex operations scales with $T_{\text{prop}} M_{\text{tot}}$. On the other hand, due to the larger matrix $\mathbf{\Phi}$, the calculation of approximate gains in (15) requires $j^3 + 2j^2 T_{\text{prop}} M_{\text{sb}} + jT_{\text{prop}} M_{\text{tot}}$ operations, which is better than in the OMP, but worse than in the SW-OMP algorithm. After the iterative part of the algorithm and J estimated paths, the calculation of subcarrier gains in (20) requires additional $J^3 M_{\text{sb}} + 2J^2 T_{\text{prop}} M_{\text{sb}} + JT_{\text{prop}} M_{\text{tot}}$ operations, which are not present in other two algorithms.

V. CONCLUSIONS

In this work, we designed a frequency-domain CS-based channel estimation algorithm for analog TTD arrays and showed that it outperforms related state-of-the algorithms. Due to a lower required overhead and sub-band based processing, the designed algorithm has a lower computational complexity than the state-of-the-art. It also achieves a lower channel estimation error across different SNRs because of improved properties of the corresponding sensing matrix.

Due to their inability to steer oversampled frequency-dependent beams, conventional phased arrays would require a large number of training frames to emulate the designed algorithm with per-sub-band processing and match the performance of analog TTD arrays. On the other hand, hybrid arrays based on phase shifters would require a reasonable training overhead to do so, but at the cost of a higher power consumption than analog TTD arrays with a single RF chain.

REFERENCES

[1] J. G. Andrews *et al.*, "What will 5G be?" *IEEE Journal on Selected Areas in Communications*, vol. 32, no. 6, pp. 1065–1082, June 2014.

[2] R. W. Heath, N. González-Prelcic, S. Rangan, W. Roh, and A. M. Sayeed, "An overview of signal processing techniques for millimeter wave MIMO systems," *IEEE Journal of Selected Topics in Signal Processing*, vol. 10, no. 3, pp. 436–453, 2016.

[3] J. Lee, G.-T. Gil, and Y. H. Lee, "Exploiting spatial sparsity for estimating channels of hybrid MIMO systems in millimeter wave communications," in *2014 IEEE Global Communications Conference*, 2014, pp. 3326–3331.

[4] Z. Marzi, D. Ramasamy, and U. Madhow, "Compressive channel estimation and tracking for large arrays in mm-Wave picocells," *IEEE J. Sel. Topics Signal Process.*, vol. 10, no. 3, pp. 514–527, Apr. 2016.

[5] K. Venugopal, A. Alkhateeb, N. González Prelcic, and R. W. Heath, "Channel estimation for hybrid architecture-based wideband millimeter wave systems," *IEEE Journal on Selected Areas in Communications*, vol. 35, no. 9, pp. 1996–2009, 2017.

[6] J. Rodríguez-Fernández, N. González-Prelcic, K. Venugopal, and R. W. Heath, "Frequency-domain compressive channel estimation for frequency-selective hybrid millimeter wave MIMO systems," *IEEE Trans. Wireless Commun.*, vol. 17, no. 5, pp. 2946–2960, 2018.

[7] Z. Gao, C. Hu, L. Dai, and Z. Wang, "Channel estimation for millimeter-wave massive MIMO with hybrid precoding over frequency-selective fading channels," *IEEE Communications Letters*, vol. 20, no. 6, pp. 1259–1262, 2016.

[8] Y. Wang, W. Xu, H. Zhang, and X. You, "Wideband mmWave channel estimation for hybrid massive MIMO with low-precision ADCs," *IEEE Wireless Communications Letters*, vol. 8, no. 1, pp. 285–288, 2019.

[9] A. Liao, Z. Gao, H. Wang, S. Chen, M.-S. Alouini, and H. Yin, "Closed-loop sparse channel estimation for wideband millimeter-wave full-dimensional MIMO systems," *IEEE Transactions on Communications*, vol. 67, no. 12, pp. 8329–8345, 2019.

[10] E. Vlachos, G. C. Alexandropoulos, and J. Thompson, "Wideband MIMO channel estimation for hybrid beamforming millimeter wave systems via random spatial sampling," *IEEE Journal of Selected Topics in Signal Processing*, vol. 13, no. 5, pp. 1136–1150, 2019.

[11] H. Yan, V. Boljanovic, and D. Cabric, "Wideband millimeter-wave beam training with true-time-delay array architecture," in *2019 53rd Asilomar Conf. Signals, Systems, Computers*, 2019, pp. 1447–1452.

[12] V. Boljanovic *et al.*, "Fast beam training with true-time-delay arrays in wideband millimeter-wave systems," *IEEE Transactions on Circuits and Systems I: Regular Papers*, vol. 68, no. 4, pp. 1727–1739, 2021.